

Commun. Theor. Phys. **76** (2024) 035004 (9pp) https://doi.org/10.1088/1572-9494/ad260e

An adaptive energy regulation in a memristive map linearized from a circuit with two memristive channels

Feifei Yang[1,2], **Ping Zhou**[1] **and Jun Ma**[1,3,*]

[1] School of Science, Chongqing University of Posts and Telecommunications, Chongqing 430065, China
[2] College of Electrical and Information Engineering, Lanzhou University of Technology, Lanzhou 730050, China
[3] Department of Physics, Lanzhou University of Technology, Lanzhou 730050, China

E-mail: hyperchaos@lut.edu.cn

Received 28 December 2023, revised 4 February 2024
Accepted for publication 5 February 2024
Published 1 March 2024

Abstract

Nonlinear circuits can show multistability when a magnetic flux-dependent memristor (MFDM) or a charge-sensitive memristor (CSM) is incorporated into a one branch circuit, which helps estimate magnetic or electric field effects. In this paper, two different kinds of memristors are incorporated into two branch circuits composed of a capacitor and a nonlinear resistor, thus a memristive circuit with double memristive channels is designed. The circuit equations are presented, and the dynamics in this oscillator with two memristive terms are discussed. Then, the memristive oscillator is converted into a memristive map by applying linear transformation on the sampled time series for the memristive oscillator. The Hamilton energy function for the memristive oscillator is obtained by using the Helmholtz theorem, and it can be mapped from the field energy of the memristive circuit. An energy function for the dual memristive map is suggested by imposing suitable weights on the discrete energy function. The dynamical behaviors of the new memristive map are investigated, and an adaptive law is proposed to regulate the firing mode in the memristive map. This work will provide a theoretical basis and experimental guidance for oscillator-to-map transformation and discrete map energy calculation.

Keywords: Hamilton energy, dual memristive map, adaptive energy regulation

(Some figures may appear in colour only in the online journal)

1. Introduction

The conceptional proposal of a memristor [1], the fabrication of a memristor [2] and its potential application have been widely explored in the control of a nonlinear circuit [3–5], neuromorphic computing [6–8], chaotic systems [9–11], and artificial neural networks [12–15]. In fact, a memristor can be embedded into a nonlinear circuit to develop a memristive circuit for presenting rich complex dynamical characteristics. For example, Yang *et al* [16] designed a simple chaotic circuit by coupling a magnetic flux-controlled memristor (MFCM) with two capacitors and an inductor. The memristive circuit has a complex hyperchaotic phenomenon and the parameter range for the chaotic region is large. Dou *et al* [17] proposed an RC bridge oscillatory circuit based on a memristor, and this memristive circuit can result in symmetric coexistence such as single-scroll, asymmetrical single-scroll, symmetric double-scroll and asymmetrical limit–cycle behaviors. Zhou *et al* [18] developed a new memristive chaotic system for inducing multistability. In addition, memristive functional neuron models [19–21] are obtained by connecting memristors into a simple neural circuit.

Recently, discrete memristors (DM) have become a research hotspot. DM's have some advantages such as low power consumption, programmability and anti-interference. Therefore, they have potential applications in the design of DM chaotic/hyperchaotic maps [22–24], neural networks [25–27] and embedded system development [28] fields.

* Author to whom any correspondence should be addressed.

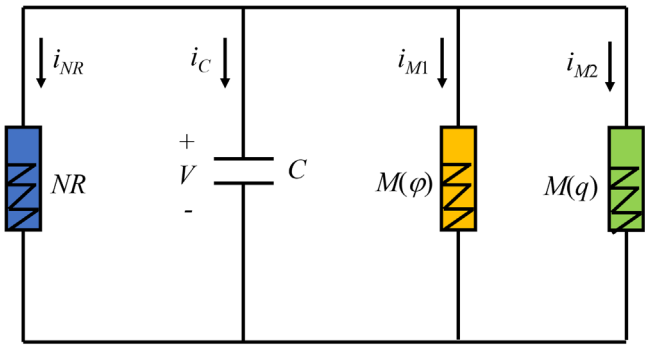

Figure 1. Schematic diagram for a dual memristive circuit. $M(\varphi)$ denotes mem-conductance for a MFCM and $M(q)$ represents mem-resistance for a CCM, respectively. C and NR means a capacitor and a nonlinear resistor, respectively.

Furthermore, a variety of DM maps have been proposed for a dynamical approach and application in signal processing. For instance, Zhang *et al* [29, 30] proposed dual memristor hyperchaotic maps from mathematical assumption. Bao *et al* [31] designed a parallel bi-memristor hyperchaotic map. The discrete memristive Rulkov neuron map [32, 33] was developed by introducing a DM into a Rulkov neuron model. A fractional memristive map is proposed in [34]. In addition, DM chaotic maps are hardware implemented by applying DSP platform [35–37] and an analog circuit [38]. One important application is that DM chaotic maps are used in image encryption algorithms [39–41].

Most of the previous works about the approach of DM maps suggested that a DM map can be defined by introducing a DM into an existing discrete map. In fact, this kind of description is artificial and is a mathematical assumption without clarifying its inner physical property. The physical modeling of a DM map is not perfect, and the energy of a DM map is also an open problem. Inspired by the suggestion in [42], biophysical and memristive maps can be converted from memristive circuits, in which the energy function for its equivalent memristive oscillator is defined in a theoretical way. In this work, a dual memristive circuit is constructed by using two different memristor elements, a nonlinear resistor and a capacitor. The dual memristive oscillator is derived and its Hamilton energy function is obtained from physical approach. According to the transformation relationship between the oscillator and the map described in [43], the dual memristive map and the corresponding Hamilton energy function are obtained. The results provide further possible guidance for designing discrete maps and calculating their energy.

This study is organized as follows: in section 2, the dual DM map is obtained. The numerical investigations are given in section 3. In section 4, the results are summarised.

2. Model and scheme

Due to the nonlinear properties of the memristor, the dynamics of a nonlinear circuit coupled by the memristor and the memristive circuit become more controllable. In this paper, a memristive circuit is constructed by including a MFCM and a CCM in two additive branch circuits, a nonlinear resistor and a capacitor are coupled in parallel in figure 1.

In figure 1, the current of the nonlinear resistance (NR) can be estimated by

$$i_{\mathrm{NR}} = -\frac{r}{\rho}\left(V - \frac{V^2}{V_0}\right). \tag{1}$$

where ρ is the resistance within the linear region, V_0 denotes a cut-off voltage and r means a dimensionless gain. V is the across voltage of the nonlinear resistor, and the dependence of voltage on the memristive channels current for the MFCM and CCM is defined by

$$\begin{cases} i_{M1} = M(\varphi)V_{M1} = \varphi V; \ \dfrac{\mathrm{d}\varphi}{\mathrm{d}t} = a\varphi + bV; \\ V_{M2} = M(q)i_{M2} = \mathrm{csc}q \cdot i_{M2}; \ \dfrac{\mathrm{d}q}{\mathrm{d}t} = \mathrm{d}q + i_{M2}. \end{cases} \tag{2}$$

As shown in equation (2), the $M(\varphi)$ and $M(q)$ have simple forms with low order, and their internal state equations are only composed of linear terms. Compared with higher-order memristors, the memristors in this paper are easier to implement physically. Sinusoidal stimulus $A\sin(2\pi\omega t)$ is imposed on the memristor, where A means the amplitude of stimulus, and ω denotes the frequency of the stimulus. The v–i curve for the MFCM with different frequencies ω under $A = 3$ is shown in figure 2(a), the v–i curve for the MFCM with different amplitudes A at $\omega = 0.8$ is shown in figure 2(b).

Figure 2 shows that the v–i curve for the MFCM is 8-shaped. The 8-shaped area decreases when the frequency of the stimulus is increased. While the 8-shaped area increases when the amplitude of the stimulus is increased. By applying the same sinusoidal stimulus $A\sin(2\pi\omega t)$, the i–v curve for the CCM with different stimuli are displayed in figure 3.

The results in figure 3 confirm that the i–v curve for the CCM exhibits a similar 8-shaped characteristic. The 8-shaped area becomes larger with the increase of amplitude and frequency of the stimulus. According to Kirchhoff's laws, the circuit equations for the memristive circuit in figure 1 are described by

$$\begin{cases} C\dfrac{\mathrm{d}V}{\mathrm{d}t} = \dfrac{r}{\rho}\left(V - \dfrac{V^2}{V_0}\right) - \varphi V - \ \sin(q)V; \\ \dfrac{\mathrm{d}\varphi}{\mathrm{d}t} = a\varphi + bV; \\ \dfrac{\mathrm{d}q}{\mathrm{d}t} = \mathrm{d}q + \ \sin(q)V. \end{cases} \tag{3}$$

To facilitate the analysis, dimensionless parameters and variables in equation (3) are defined as follows

$$\begin{cases} x = \dfrac{V}{V_0}, \ w = \dfrac{\varphi}{\rho C V_0}, \ u = \dfrac{q}{CV_0}, \ \tau = \dfrac{t}{\rho C}, \ a = \rho^2 C V_0, \\ c = a\rho C, \ \alpha = \rho, \ k = CV_0, \ \mathrm{d}' = \mathrm{d}C\rho. \end{cases} \tag{4}$$

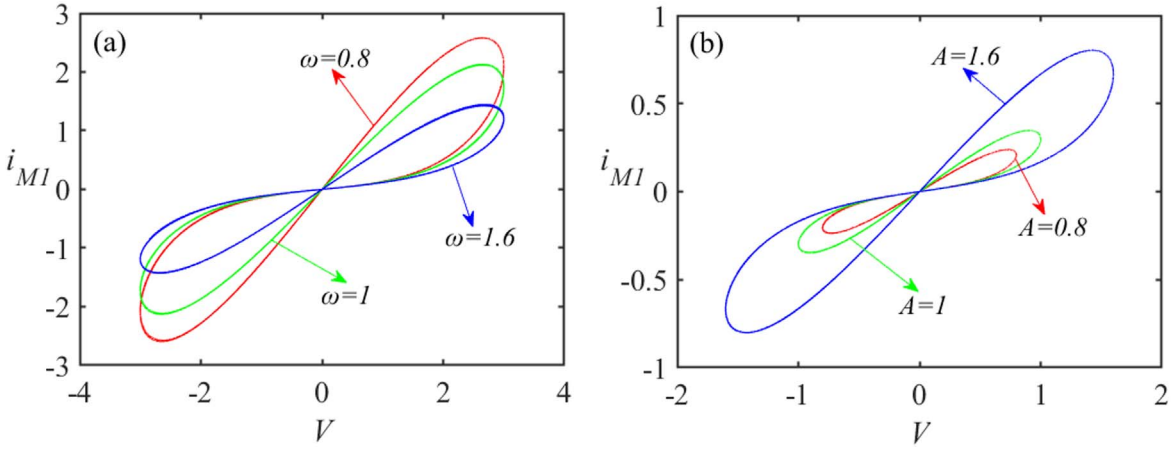

Figure 2. The *v*–*i* curve for the MFCM with different stimuli. For (a) $A = 3$; (b) $\omega = 0.8$.

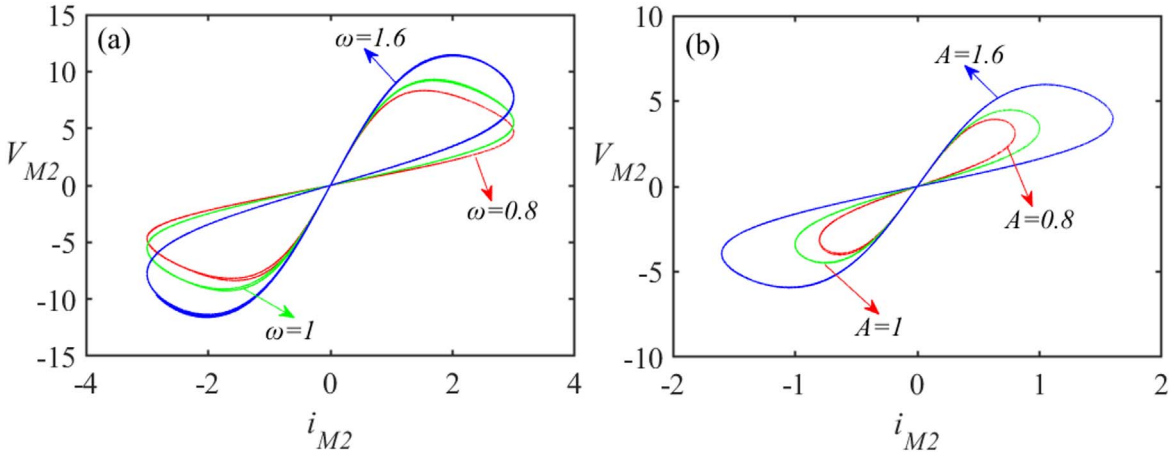

Figure 3. The *i*–*v* curve for the MFCM with different stimuli. For (a) $A = 3$; (b) $\omega = 0.8$.

The dynamic equations in equation (3) can be rewritten by

$$\begin{cases} \dfrac{\mathrm{d}x}{\mathrm{d}t} = r(x - x^2) - awx - \alpha \sin(ku)x; \\ \dfrac{\mathrm{d}w}{\mathrm{d}t} = cw + bx \ ; \\ \dfrac{\mathrm{d}u}{\mathrm{d}t} = \mathrm{d}'u + \alpha \sin(ku)x. \end{cases} \tag{5}$$

The memristive ciruit in figure 1 has three energy storage elements, the field energy W and its dimensionless Hamilton energy H are given in equation (6).

$$\begin{cases} W = \dfrac{1}{2}CV^2 + \dfrac{1}{2}\varphi i_{M1} + \dfrac{1}{2}qV; \\ H = \dfrac{W}{CV_0^2} = \dfrac{1}{2}x^2 + \dfrac{1}{2}aw^2x + \dfrac{1}{2}ux. \end{cases} \tag{6}$$

The Hamilton energy function H in equation (6) for the memristive oscillator in equation (5) can be proven by applying the Helmholtz's theorem, when the memristive oscillator in equation (5) is rewritten in a vector form

$$\begin{aligned} \begin{pmatrix} \dfrac{\mathrm{d}x}{\mathrm{d}\tau} \\ \dfrac{\mathrm{d}w}{\mathrm{d}\tau} \\ \dfrac{\mathrm{d}u}{\mathrm{d}\tau} \end{pmatrix} &= \begin{pmatrix} r(x - x^2) - awx - \alpha \sin(ku)x \\ cw + bx \\ \mathrm{d}'u + \alpha \sin(ku)x \end{pmatrix} = F_\mathrm{c} + F_\mathrm{d} \\ &= \begin{pmatrix} -abwx - \mathrm{d}'x \\ bx + 0.5abw^2 + 0.5bu \\ 2\mathrm{d}'x + a\mathrm{d}'w^2 + \mathrm{d}'u \end{pmatrix} \\ &+ \begin{pmatrix} r(x - x^2) - awx(1 - b) + \mathrm{d}'x - \alpha \sin(ku)x \\ cw - 0.5abw^2 - 0.5bu \\ -2\mathrm{d}'x - a\mathrm{d}'w^2 + \alpha \sin(ku)x \end{pmatrix} \\ &= \begin{pmatrix} 0 & -b & -2\mathrm{d}' \\ b & 0 & 0 \\ 2\mathrm{d}' & 0 & 0 \end{pmatrix} \begin{pmatrix} x + 0.5aw^2 + 0.5u \\ awx \\ 0.5x \end{pmatrix} \\ &+ \begin{pmatrix} A_{11} & 0 & 0 \\ 0 & A_{22} & 0 \\ 0 & 0 & A_{33} \end{pmatrix} \begin{pmatrix} x + 0.5aw^2 + 0.5u \\ awx \\ 0.5x \end{pmatrix}; \end{aligned}$$

$$
\begin{aligned}
&A_{11}\\
&= \frac{r(x-x^2) - awx(1-b) + d'x - \alpha\sin(ku)x}{x + 0.5aw^2 + 0.5u};\\
&A_{22} = \frac{cw - 0.5abw^2 - 0.5bu}{awx};\\
&A_{33} = \frac{-2d'x - adw^2 + \alpha\sin(ku)x}{0.5x}.
\end{aligned} \tag{7}
$$

According to the Helmholtz's theorem, the Hamilton energy function H meets the following criterion

$$
\begin{aligned}
\nabla H^{\mathrm{T}} F_{\mathrm{c}} = {} & (-abwx - \mathrm{d}'x)\frac{\partial H}{\partial x}\\
& + (bx + 0.5abw^2 + 0.5bu)\frac{\partial H}{\partial w}\\
& + (2\mathrm{d}'x + \mathrm{d}'u + a\mathrm{d}'w^2)\frac{\partial H}{\partial u} = 0.
\end{aligned} \tag{8}
$$

$$
\begin{aligned}
&\frac{\mathrm{d}H}{\mathrm{d}\tau} = [r(x-x^2) - awx(1-b) + \mathrm{d}'x\\
&- \alpha\sin(ku)x](x + 0.5aw^2 + 0.5u)\\
&+ awx(cw - 0.5abw^2 - 0.5bu)\\
&+ 0.5x[-2\mathrm{d}'x - a\mathrm{d}w^2 + \alpha\sin(ku)x] = \nabla H^{\mathrm{T}} F_{\mathrm{d}}.
\end{aligned} \tag{9}
$$

Indeed, the energy function H in equation (6) satisfies the criterion in equations (8) and (9) completely. Furthermore, linear transformation is imposed on the sampled time series for variables from equation (5) with time step $\Delta\tau$ during a numerical approach.

$$
\begin{cases}
y_n = \dfrac{r\Delta\tau}{1 + r\Delta\tau}x_n,\ z_n = \dfrac{r\Delta\tau}{1 + r\Delta\tau}w_n,\\
v_n = \dfrac{r\Delta\tau}{1 + r\Delta\tau}u_n,\ \lambda = 1 + r\Delta\tau;\\
b = \dfrac{1 + r\Delta\tau}{r},\ \beta = \alpha\Delta\tau,\ \delta = k\dfrac{1 + r\Delta\tau}{r\Delta\tau},\\
a = c\Delta\tau + 1,\ c = b\Delta\tau,\ d = d'\Delta\tau + 1.
\end{cases} \tag{10}
$$

These renewed discrete variables accompanied with updated parameters can be used to define a new memristive map as follows

$$
\begin{cases}
y_{n+1} = \lambda(y_n - y_n^2) - by_n z_n - \beta\sin(\delta v_n)y_n;\\
z_{n+1} = ay_n + cz_n;\\
v_{n+1} = dv_n + \beta\sin(\delta v_n)y_n.
\end{cases} \tag{11}
$$

Under the same weights for two terms in the discrete energy function for equation (6), the Hamilton energy for the map in equation (11) is described by

$$
H_n = \frac{1}{2}y_n + \frac{1}{2}bz_n^2 y_n + \frac{1}{2}v_n y_n. \tag{12}
$$

As suggested in the recent works [44, 45], membrane parameters or memristive parameters can be controlled by the energy flow to induce a mode transition when the inner energy level is beyond a threshold. To investigate the self-adaption in the dual memristive map, it requires that parameter a for the dual memristive map can be controlled by the energy flux in an adaptive way as follows

$$
\begin{cases}
a_{n+1} = a_n + k\cdot\theta(p - H_n),\ \theta(\cdot)\\
=1,\ p \geqslant 0,\ \theta(\cdot) = 0,\ p < 0;\\
or,\quad a = k\cdot\theta(p - H_n),\ \theta(\cdot)\\
=1,\ p \geqslant 0,\ \theta(\cdot) = 0,\ p < 0.
\end{cases} \tag{13}
$$

Where the energy threshold $0 < p < 1$ determines the energy level of a memristive map in the nth iteration. a_n denotes value for the map parameter in the nth iteration, parameter k means growth step, and the Heaviside function $\theta(^*)$ is used to control parameter growth to a saturation value.

3. Results and discussion

Similar to most of the memristive oscillators [20, 21, 46–50], numerical solutions for equation (5) can be obtained and additive noise can be applied to induce nonlinear resonance and mode control in neural activities. Numerical results are mainly explored in the memristive map under the control of adaptive law in equation (13). To investigate the complex dynamic characteristics of the dual memristive map presented in equation (11), the initial values of the memristive map are selected as (0.1, 0.1, 0). The parameters of the memristive map are fixed as $\lambda = 3.9$, $b = 0.2$, $c = 0.3$, $d = 0.4$, $\beta = 0.1$, $\delta = 0.1$. The bifurcation diagram and the Lyapunov exponents (LEs) spectrum are calculated by changing the parameter a carefully, and the results are plotted in figure 4.

The results in figure 4 show that the dual memristive map triggers a mode transition with the increase of the parameter a, such as period-1, period-2, period-4, period-8 and chaotic behaviors are generated. The positive Lyapunov exponent becomes negative and the inverse double period bifurcation occurs by increasing parameter a in a continuous way, and chaos is suppressed effectively. Furthermore, phase portraits of the memristive map with different values for parameter a are shown in figure 5.

In figure 5, the profile of the attractors shows period-2, period-4, period-8 and chaotic characteristics. According to the Hamilton energy function presented in equation (12), the relation between the Hamilton energy and the oscillatory states in the memristive map is calculated, and the results are shown in figure 6.

The results in figure 6 illustrate that the dual memristive map has a higher mean value of Hamilton energy with period state, while it has a lower mean value of Hamilton energy with a chaotic pattern. In addition, the mean value of Hamilton energy decreases with the increase of a period number.

When the parameters in equation (11) are fixed at $d = 1$ and $\delta = 1$, the memristive map exits the fixed point (0, 0, 0 $\pm h\pi$) ($h = 0, \pm1, \pm2, \pm3\ldots$), and indicates that the memristive map can be initially boosted to give extreme multistability. The parameters are $\lambda = 3.9$, $a = 0.5$, $b = 0.2$, $c = 0.3$, $d = 1$, $\beta = 0.1$, $\delta = 1$, by changing the initial value v (0), the phase portraits are shown in figure 7.

The results in figure 7 confirm that the memristive map will produce an extreme multistable phenomenon by

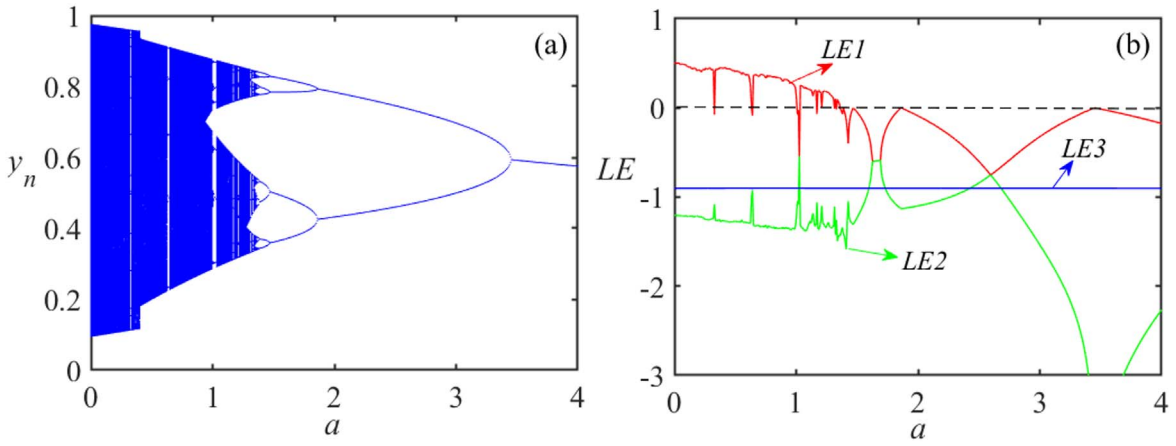

Figure 4. (a) Bifurcation diagram and (b) the distribution of the LEs for the memristive map by changing parameter a. Setting $\lambda = 3.9$, $b = 0.2$, $c = 0.3$, $d = 0.4$, $\beta = 0.1$, $\delta = 0.1$. The initial value is (0.1, 0.1, 0).

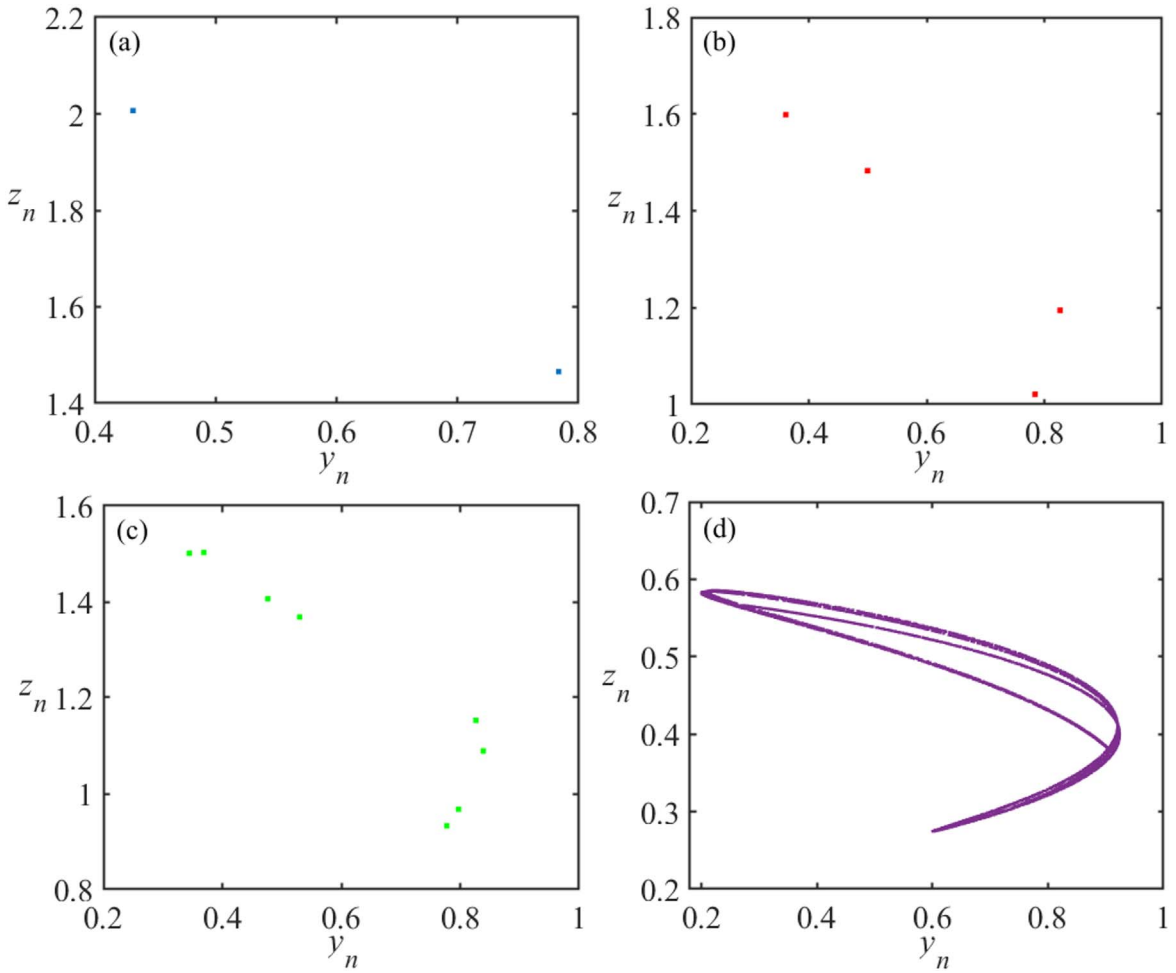

Figure 5. Phase portraits of the memristive map by changing parameter a. For (a) $a = 2$; (b) $a = 1.5$; (c) $a = 1.4$; (d) $a = 0.5$. The parameters are $\lambda = 3.9$, $b = 0.2$, $c = 0.3$, $d = 0.4$, $\beta = 0.1$, $\delta = 0.1$. The initial value is (0.1, 0.1, 0).

changing the initial value for the variable v. According to the criterion of the growth for parameter a in equation (13), it sets the threshold $p = 0.35$, parameters are fixed at $\lambda = 3.9$, $b = 0.2$, $c = 0.3$, $d = 0.4$, $\beta = 0.1$, $\delta = 0.1$, and initial values are selected as (0.1, 0.1, 0). The initial value for parameter $a = 0.5$, gains $k = 0.005$ and $k = 0.007$, the memristive map in equation (11) is iterated 1200 times, respectively. The growth of parameter a, changes of Hamilton energy and phase diagram are shown in figure 8.

It is confirmed that parameter a of the memristive map relative to when the MFCM reaches a stable value of 2.39 after 800 iterations. The Hamilton energy shows a distinct

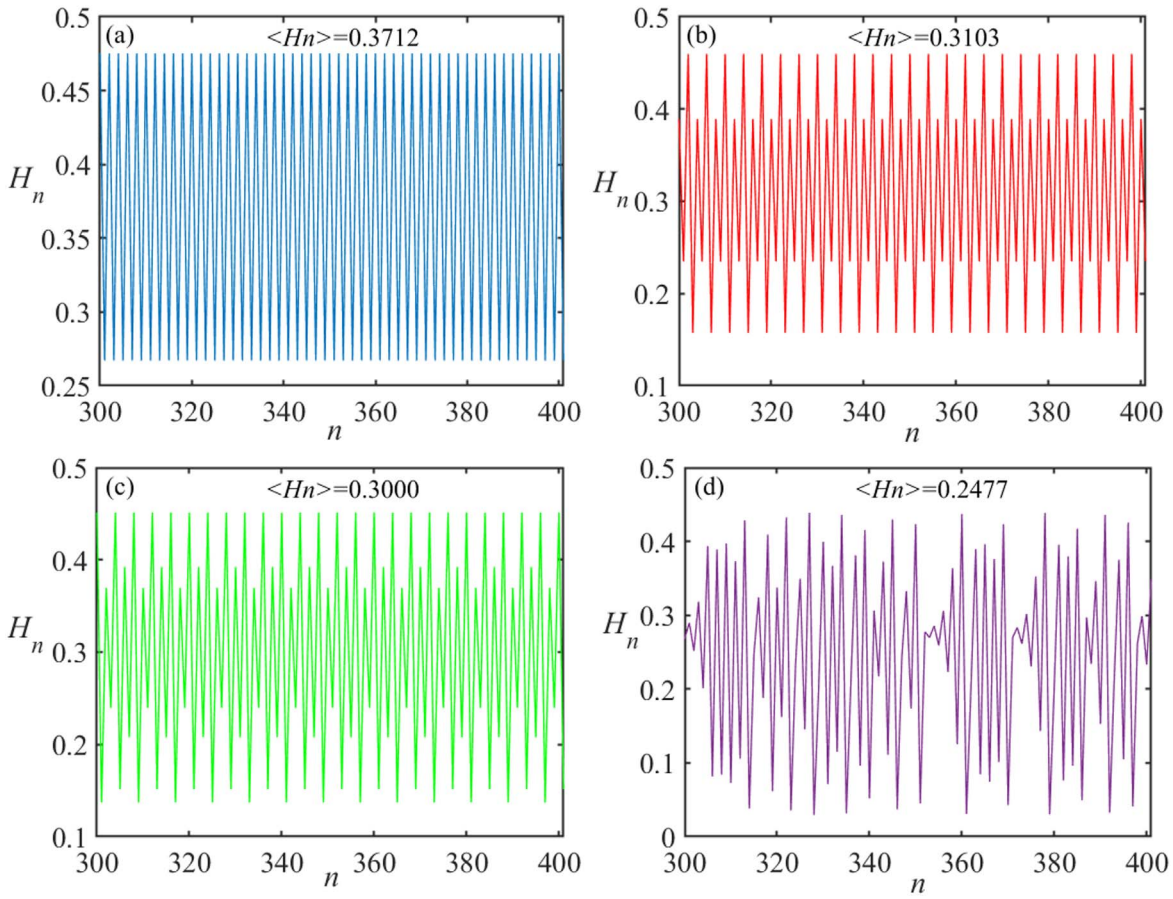

Figure 6. Evolution of energy function and its average value in the memristive map by changing parameter a. For (a) $a = 2$; (b) $a = 1.5$; (c) $a = 1.4$; (d) $a = 0.5$. Setting $\lambda = 3.9$, $b = 0.2$, $c = 0.3$, $d = 0.4$, $\beta = 0.1$, $\delta = 0.1$. The initial value is (0.1, 0.1, 0). $<H_n>$ denotes the average value of the Hamilton energy.

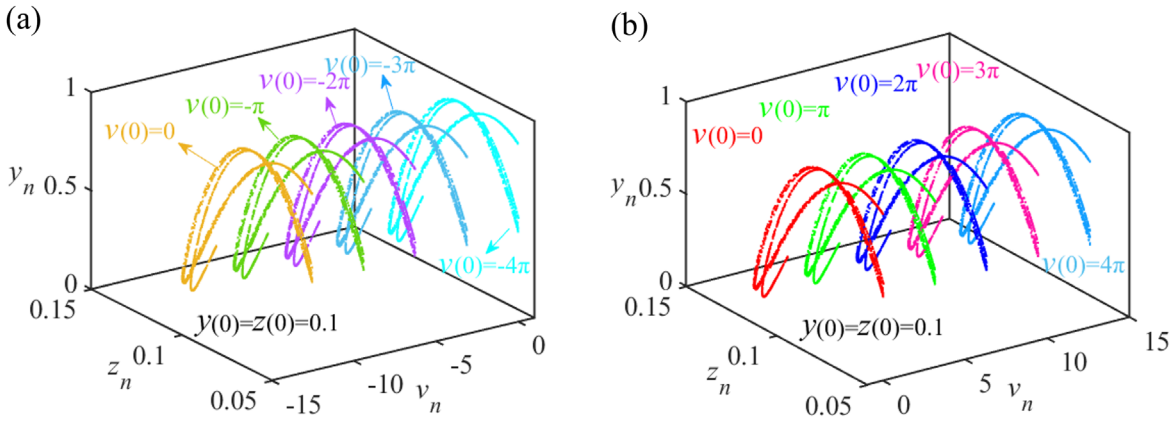

Figure 7. Phase portraits of the memristive map by changing initial value $v(0)$. For (a) initial value is (0.1, 0.1, 0-$h\pi$), ($h = 0$, 1, 2, 3, 4); (b) initial value is (0.1, 0.1, 0+$h\pi$), ($h = 0$, 1, 2, 3, 4). The parameters are $\lambda = 3.9$, $a = 0.5$, $b = 0.2$, $c = 0.3$, $d = 1$, $\beta = 0.1$, $\delta = 1$.

transition when the memristive maps change the chaotic patterns to periodic states, and a similar shift occurs in the phase diagram. By comparing figures 8(a) and (b), it is found that with the increased value of gain k, parameter a needs fewer iterations to reach a saturation value. The result indicates that the dynamics for the memristive map can be controlled by the energy flow in an adaptive way. Considering that the chaotic systems are extremely sensitive to the parameters and initial values, the map attractor basins on $y(0)$-$v(0)$ and $z(0)$-$v(0)$ are shown in figure 9.

It is found that the initial values affect the chaotic region (blue region) and the periodic region (red region) at different initial values. As a result, the stochastic and continuous switch of the initial values for the memristive variables will induce a distinct mode transition and energy shift.

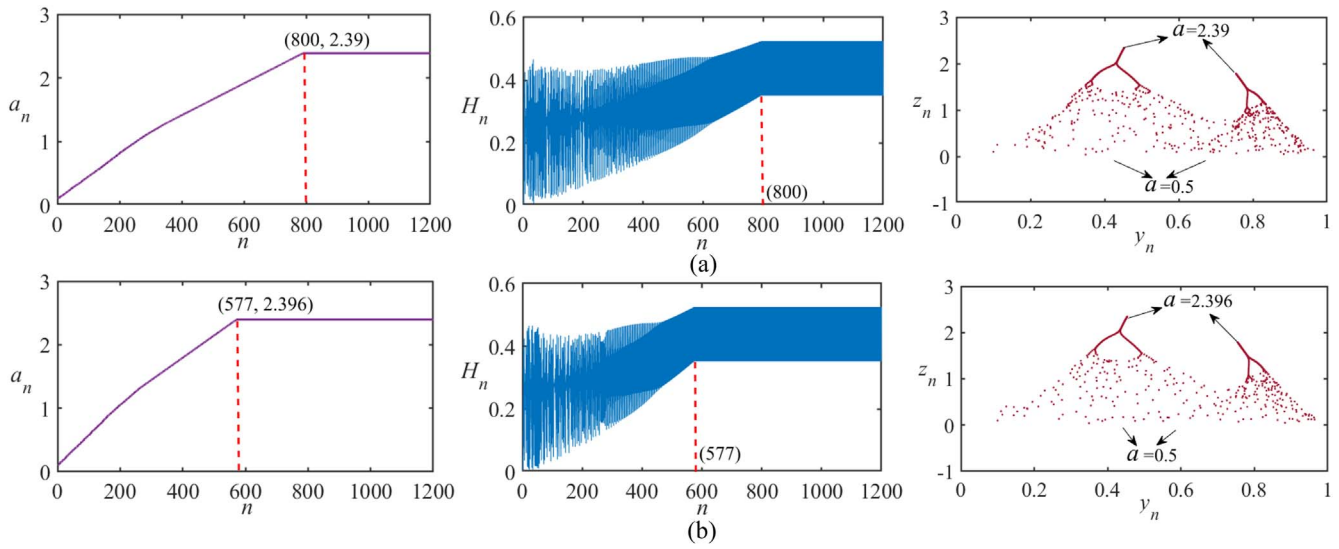

Figure 8. Growth of parameter a, Hamilton energy and phase diagram for gain k. For (a) $k = 0.005$; (b) $k = 0.007$. Setting $\lambda = 3.9$, $b = 0.2$, $c = 0.3$, $d = 0.4$, $\beta = 0.1$, $\delta = 0.1$. Setting initial values for variables (0.1, 0.1, 0).

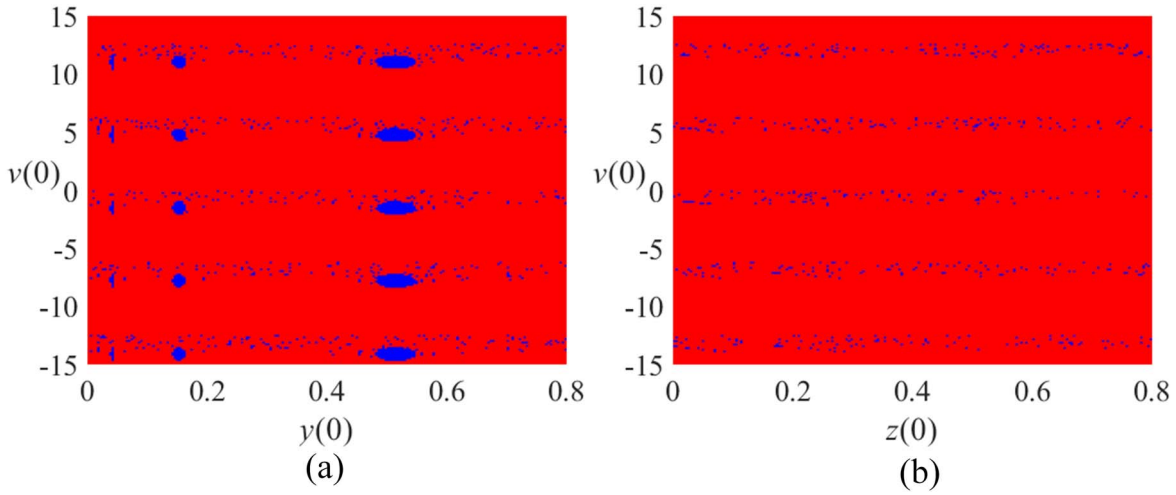

Figure 9. Map attractor basins on the plane. For (a) initial value ($y(0)$, 0.1, $v(0)$); (b) initial value (0.1, $z(0)$, $v(0)$). Setting $\lambda = 3.9$, $b = 0.2$, $c = 0.3$, $d = 0.4$, $\beta = 0.1$, $\delta = 0.1$, $a = 0.5$.

From the memristive oscillator in equation (5) to the memristive map in equation (11), perfect covariance in the formulas is confirmed. The continuous energy function in equation (6) is relative to the state variables and bifurcation parameter a directly, while the discrete energy function for the map in equation (12) is dependent on the discrete variables and parameter b completely. From a dynamical viewpoint, the energy level for both the memristive oscillator and the memristive map can be calculated by adjusting one bifurcation parameter carefully. In fact, the two curves for the energy function in the oscillator and the map seldom intersect, keeping the same energy value due to the involvement of the time step when the memristive oscillator is obtained with numerical solutions. In an experimental approach, analog signals from the nonlinear circuit can be filtered and adjusted to present discrete signals, and the memristive map provides fast computing without further estimating the time step. Our scheme provides a reference to verify the reliability of the mathematical maps. As a result, these physical maps can be connected to build an artificial array for signal processing in parallel.

4. Conclusion

In this paper, a dual memristive circuit is built to develop a memristive oscillator for discerning the effect of the magnetic field and the electric field synchronously. The energy function for the dual memristive oscillator is obtained in a theoretical way. By applying a linear transformation on the sampled variables for the memristive oscillator, a dual memristive map is designed with a clear definition of the energy function and adaptive growth law for one bifurcation parameter. The results indicate that the dual memristive map has rich dynamical behaviors, and the dynamics can be adjusted in an adaptive way under energy flow. The memristive map has a

smaller average Hamilton energy value in the chaotic state, while it prefers to keep a higher mean Hamilton energy value in the periodic state. In addition, the mean Hamilton energy value of the memristive map decreases with the increase of the period number. The results confirm the reliability of discrete maps from nonlinear circuits. The modeling method of the discrete map proposed in this paper can be applied to other high-dimensional discrete maps including discrete memristive maps and neurons. The Hamilton energy calculation and adaptive control method can be applied to the energy calculation and the adaptive control of other discrete scatter maps. In addition, the simplest map proposed in this paper can be used for pseudo-random sequence generators and image encryption fields.

Acknowledgments

This study is strongly supported by the National Science Foundation of China under Grant No. 12072139.

CRediT authorship contribution statement

FY Methodology, software, numerical calculation, **PZ** and **JM** Methodology, supervision, formal analysis, writing-final version.

Declaration of competing interest

We declare that all of the authors have no competing financial interests or personal relationships for the work reported in this study.

References

[1] Chua L 1971 Memristor-the missing circuit element *IEEE Trans. Circuit Theory* **18** 507–19
[2] Strukov D B *et al* 2008 The missing memristor found *Nature* **453** 80–3
[3] Fouda M E, Elwakil A S and Radwan A G 2015 Pinched hysteresis with inverse-memristor frequency characteristics in some nonlinear circuit elements *Microelectron. J.* **46** 834–8
[4] Corinto F, Ascoli A and Gilli M 2011 Nonlinear dynamics of memristor oscillators *IEEE Trans. Circuits Syst. I* **58** 1323–36
[5] Bao B *et al* 2017 Two-memristor-based Chua's hyperchaotic circuit with plane equilibrium and its extreme multistability *Nonlinear Dyn.* **89** 1157–71
[6] Indiveri G *et al* 2013 Integration of nanoscale memristor synapses in neuromorphic computing architectures *Nanotechnology* **24** 384010
[7] Hu M *et al* 2014 Memristor crossbar-based neuromorphic computing system: a case study *IEEE Trans Neural Netw. Learn. Syst.* **25** 1864–78
[8] Wang Z *et al* 2017 Memristors with diffusive dynamics as synaptic emulators for neuromorphic computing *Nat. Mater.* **16** 101–8
[9] Lai Q *et al* 2020 Coexisting attractors, circuit implementation and synchronization control of a new chaotic system evolved from the simplest memristor chaotic circuit *Commun. Nonlinear Sci. Numer. Simul.* **89** 105341
[10] Sun J *et al* 2018 Autonomous memristor chaotic systems of infinite chaotic attractors and circuitry realization *Nonlinear Dyn.* **94** 2879–87
[11] Messadi M *et al* 2023 A new 4D memristor chaotic system: analysis and implementation *Integration* **88** 91–100
[12] Ntinas V *et al* 2018 Experimental study of artificial neural networks using a digital memristor simulator *IEEE Trans Neural Netw. Learn. Syst.* **29** 5098–110
[13] Wang W *et al* 2019 A self-rectification and quasi-linear analogue memristor for artificial neural networks *IEEE Electron Device Lett.* **40** 1407–10
[14] Zhang Z *et al* 2023 An FPGA-based memristor emulator for artificial neural network *Microelectron. J.* **131** 105639
[15] Park S O *et al* 2023 Linear conductance update improvement of CMOS-compatible second-order memristors for fast and energy-efficient training of a neural network using a memristor crossbar array *Nanoscale Horizons* **8** 1366–76
[16] Yang G, Zhang X and Moshayedi A J 2023 Implementation of the simple hyperchaotic memristor circuit with attractor evolution and large-scale parameter permission *Entropy* **25** 203
[17] Dou G *et al* 2023 RC bridge oscillation memristor chaotic circuit for electrical and electronic technology extended simulation experiment *Micromachines* **14** 410
[18] Zhou Z and Ye X 2023 Generating rotationally hidden attractive sea via a new chaotic system with two mixed memristors *Phys. Scr.* **98** 095237
[19] Yang F, Xu Y and Ma J 2023 A memristive neuron and its adaptability to external electric field *Chaos* **33** 023110
[20] Yang F, Ren G and Tang J 2023 Dynamics in a memristive neuron under an electromagnetic field *Nonlinear Dyn.* **111** 21917–39
[21] Hou B *et al* 2023 Energy flow and stochastic resonance in a memristive neuron *Phys. Scr.* **98** 105236
[22] Laskaridis L *et al* 2023 Study of the dynamical behavior of an Ikeda-based map with a discrete memristor *Integration* **89** 168–77
[23] Ma Y *et al* 2023 A discrete memristor coupled two-dimensional generalized square hyperchaotic maps *Fractals* **31** 2340136
[24] Xu B *et al* 2023 A 3D discrete memristor hyperchaotic map with application in dual-channel random signal generator *Chaos, Solitons Fractals* **173** 113661
[25] Lai Q and Yang L 2023 Discrete memristor applied to construct neural networks with homogeneous and heterogeneous coexisting attractors *Chaos, Solitons Fractals* **174** 113807
[26] Xiao Q, Huang Z and Zeng Z 2017 Passivity analysis for memristor-based inertial neural networks with discrete and distributed delays *IEEE Trans. Systems, Man, Cybernetics: Systems 2017* **49** 375–85
[27] Shang C *et al* 2023 Spatial patterns and chimera states in discrete memristor coupled neural networks *Nonlinear Dyn.* **111** 20347–60
[28] Tolba M F *et al* 2018 Memristor FPGA IP core implementation for analog and digital applications *IEEE Trans. Circuits Systems II: Express Briefs 2018* **66** 1381–5
[29] Zhang S, Zhang H and Wang C 2023 Dynamical analysis and applications of a novel 2D hybrid dual-memristor hyperchaotic map with complexity enhancement *Nonlinear Dyn.* **111** 15487–513
[30] Zhang S, Zhang H and Wang C 2023 Memristor initial-boosted extreme multistability in the novel dual-memristor hyperchaotic maps *Chaos, Solitons Fractals* **174** 113885
[31] Bao H *et al* 2022 Parallel bi-memristor hyperchaotic map with extreme multistability *Chaos, Solitons Fractals* **160** 112273

[32] Li Y *et al* 2023 Offset boosting-entangled complex dynamics in the memristive Rulkov neuron *IEEE Trans. Ind. Electron.* (https://doi.org/10.1109/TIE.2023.3325558)
[33] Bao H *et al* 2023 Memristive effects on an improved discrete Rulkov neuron model *Sci. China Technol. Sci.* **66** 3153–63
[34] Shatnawi M T *et al* 2023 Hidden multistability of fractional discrete non-equilibrium point memristor based map *Phys. Scr.* **98** 035213
[35] Ma Y *et al* 2023 Design and DSP implementation of a hyperchaotic map with infinite coexisting attractors and intermittent chaos based on a novel locally active memcapacitor *Chaos, Solitons Fractals* **173** 113708
[36] Qin C, Sun K and He S 2021 Characteristic analysis of fractional-order memristor-based hypogenetic jerk system and its DSP implementation *Electronics* **10** 841
[37] Ma T *et al* 2023 Hidden dynamics of memristor-coupled neurons with multi-stability and multi-transient hyperchaotic behavior *Phys. Scr.* **98** 105202
[38] Fu L *et al* 2023 A memristive Hénon map based on the state variable difference and its analog circuit implementation *IEEE Trans. Ind. Electron.* (https://doi.org/10.1109/TIE.2023.3292857)
[39] Lai Q, Liu Y and Yang L 2023 Image encryption using memristive hyperchaos *Appl. Intel.* **53** 22863–81
[40] Zhu L *et al* 2022 A visually secure image encryption scheme using adaptive-thresholding sparsification compression sensing model and newly-designed memristive chaotic map *Inf. Sci.* **607** 1001–22
[41] Peng Y *et al* 2023 A simple color image encryption algorithm based on a discrete memristive hyperchaotic map and time-controllable operation *Opt. Laser Technol.* **165** 109543
[42] Ma J 2024 Energy function for some maps and nonlinear oscillators *Appl. Math. Comput.* **463** 128379
[43] Guo Y T, Xie Y and Ma J 2023 How to define energy function for memristive oscillator and map *Nonlinear Dyn.* **111** 21903–15
[44] Wu F Q, Guo Y T and Ma J 2023 Energy flow accounts for the adaptive property of functional synapses *Sci. China Technol. Sci.* **66** 3139–52
[45] Guo Y *et al* 2023 Physical approach of a neuron model with memristive membranes *Chaos* **33** 113106
[46] Fonzin T F *et al* 2018 Coexisting bifurcations in a memristive hyperchaotic oscillator *AEU Int. J. Electron. Commun.* **90** 110–22
[47] Bao B C *et al* 2018 Symmetric periodic bursting behavior and bifurcation mechanism in a third-order memristive diode bridge-based oscillator *Chaos, Solitons Fractals* **109** 146–53
[48] Sahin M E *et al* 2020 Design of a hyperchaotic memristive circuit based on Wien bridge oscillator *Comput. Electr. Eng.* **88** 106826
[49] Fonzin Fozin T *et al* 2019 Control of multistability in a self-excited memristive hyperchaotic oscillator *Int. J. Bifurcation Chaos* **29** 1950119
[50] Li R *et al* 2022 A new autonomous memristive megastable oscillator and its Hamilton-energy-dependent megastability *Chaos* **32** 013127